Journal of the Ceramic Society of Japan 130 [9] 807-815 2022
DOI http://doi.org/10.2109/jcersj2.22051

JCS-Japan

FULL PAPER

Reaction of $CaSi_2$ and $FeCl_2$ with additional NaCl to synthesis of β-$FeSi_2$/Si composites

Ye Li[1,†], Jilani Ansari[2], Yosuke Shimura[2,3,‡], Hirokazu Tatsuoka[2] and Liugang Chen[4]

[1]Graduate School of Science and Technology, Shizuoka University, Hamamatsu 432–8011, Japan
[2]Graduate School of Integrated Science and Technology, Shizuoka University, Hamamatsu 432–8561, Japan
[3]Research Institute of Electronics, Shizuoka University, Hamamatsu 432–8011, Japan
[4]Henan Key Laboratory of High Temperature Functional Ceramics, School of Materials Science and Engineering, Zhengzhou University, Zhengzhou, Henan 450001, China

This work studied the impact of the molar ratio of $CaSi_2$ and $FeCl_2$ and additional NaCl under Ar atmosphere on the formation of β-$FeSi_2$/Si composites. Phase and microstructure of silicide were characterized by X-ray powder diffraction (XRD), scanning electron microscopy (SEM) and transmission electron microscopy (TEM), respectively. The results indicate that the formation of β-$FeSi_2$ was favored in the sample with a molar ratio of $CaSi_2/FeCl_2$ higher than 1 while β-$FeSi_2$ was not generated in the sample with a molar ratio of $CaSi_2/FeCl_2$ equal to 1. β-$FeSi_2$/Si composites, β-$FeSi_2$ growing on the surface of Si nanosheet bundles and the surface of Si nanosheets, were formed in the sample with a 1:0.5:2.2 molar ratio of $CaSi_2$, $FeCl_2$, and NaCl.

Key-words : β-$FeSi_2$/Si composites, Silicide, Phase, Microstructure

[Received March 23, 2022; Accepted July 4, 2022]

1. Introduction

Due to the enhanced optical and electrical properties, and physical properties such as surface area compared to those of the bulk materials, low-dimensional nanostructured materials have been widely studied for various field areas of science such as sensing devices,[1)–3)] catalysis[4),5)] and energy storage devices.[6)–9)]

Recently, various Si-based nanosheets or nanocomposites, which present modified optical properties and/or have excellent anode performance as lithium-ion (Li-ion) battery electrodes, have been synthesized by the solid-state reactions of $CaSi_2$ and metal chlorides.[6),7),10)–14)] Oh et al.[7)] synthesized various Si-based nanocomposites consisting of nanoflake-like Ca_xSi_2 particles and transition metal silicide (MSi_y; M: Ni, Fe or Mn) particles by heating $CaSi_2$ and metal (M) chlorides mixture in a sealed stainless-steel tube at 600 °C. Itahara et al.[12)] prepared fine Mg_2Si/Si composite powders by the reaction of $CaSi_2$, $MgCl_2$, and Na at 650 °C. These fine Si-based composites exhibited good anode performance in Li-ion batteries.[7),10)–12)] A calcium-bridged siloxane consisting of Ca-bridged and fragmented Si planes was obtained by a solid-state reaction of $CaSi_2$ and $TaCl_5$ at 215 °C, which shows tunable optical properties as well as stable Li-ion battery anode performance.[6),13)] Additionally, Mg_2Si/Si composites containing Si nanosheet bundles and Mg_2Si deposits were synthesized via heating treatment $CaSi_2$ and $MgCl_2$ mixture in a sealed stainless-steel cell under Ar atmosphere at 650 °C.[14)] The prepared Mg_2Si/Si composites affect the emission property of the Si nanosheets.[14)] Therefore, the reaction of $CaSi_2$ and transition metal chlorides mixture is an effective method to acquire various Si-based nanosheets or nanocomposites.

$FeSi_x$/Si ($FeSi_x$: FeSi and α-$FeSi_2$) composites, as potential material for Li-ion battery anode, have been widely studied in recent years.[15)–18)] These $FeSi_x$/Si composites synthesized by mechanical alloying method are composed of nanosized particles and exhibit excellent performance in Li-ion battery anode. This can be attributed to two main reasons. First, $FeSi_x$ around Si could effectively buffer the volumetric change of the electrodes and then improve the cycling stability of the composite material.[16)–18)] Second, $FeSi_x$ could effectively improve the electrical conductivity of electrodes because the electrical resistance of $FeSi_x$ (FeSi and α-$FeSi_2$) and Si is 2.6×10^1 and 6.0×10^3 Ω cm, respectively.[18)] Liu et al.[19)] stated that nanosheets often have large exposed surfaces and specific facets when compared with nanoparticles, making them more attractive in energy devices. Tani et al.[20)] reported that the electrical resistivity of β-$FeSi_2$ is 1.38×10^1 Ω cm, which is slightly higher than the electrical resistance of FeSi and α-$FeSi_2$ (2.6×10^1 Ω cm).[18)] Therefore, it is expected that β-$FeSi_2$/

† Corresponding author: Y. Li; E-mail: li.ye.19@shizuoka.ac.jp
‡ Present address: imec, Kapeldreef 75, 3001 Leuven, Belgium

Si composites containing nanosheet bundles could be synthesized and exhibit enhanced anode performance in Li-ion batteries. Additionally, because of the possible enhancement of the thermoelectromotive force by the quantum confinement effect,[21] it is also expected that fine β-$FeSi_2$/Si composites containing nanosheet bundles could be used as the raw material for the nanostructured thermoelectric bulk materials. Itahara et al.[10] reported that Si-based composites containing iron silicide (FeSi and Fe_3Si) particles and Ca–Si or Si nanosheet bundles have been synthesized by the solid-state reaction of $CaSi_2$ and $FeCl_2$ mixture and presented good anode performance in Li-ion batteries. It is expected that β-$FeSi_2$/Si composites could be synthesized based on the reaction of $CaSi_2$ and $FeCl_2$. The phase nucleation, phase sequence or phase selection for the formation of iron silicide have been intensively investigated between the metal and silicon diffusion couple. For example, Zhang et al.[22] found that Fe_3Si was initially formed between the bulk diffusion couple of Fe–Si at 700 °C. Walser et al.[23] reported that the first nucleation phase between Fe–Si thin film was FeSi. They discussed the formation of FeSi based on a combination of thermodynamic and kinetic considerations, which was also used to discuss the formation of other silicide nanostructures.[24] However, the formation of β-$FeSi_2$ is usually very difficult and takes a very long time, which is related to the large nucleation barrier of β-$FeSi_2$.[25),26]

Yamada et al.[27] synthesized β-$FeSi_2$ powder by annealing the Fe and Si mixture in Na melt at 500–800 °C under an Ar atmosphere and explained that the formation of β-$FeSi_2$ powder is because Si dissolved in the Na melt react with Fe powder. In addition, various silicide powder, such as α-$MoSi_2$ and β-$MoSi_2$,[28] β-SiC,[29] $CrSi_2$, $MnSi_{1.7+\delta}$, and CoSi[30] have been prepared using Na melt/flux at low temperature, which is also due to the reaction of Si dissolved in Na melt and metal powder. These researches suggest that Si dissolved in Na melt probably has higher activity. Harada et al.[31] found Si material can be prepared by the reaction of $CaSi_2$ and NaCl according to the reaction formula: $CaSi_2 + NaCl \rightarrow 2Si + CaCl_2 + 2Na$ and stated that the generated Na dissolves rapidly in the molten salt containing NaCl and the side reaction between Na and Si probably hardly occurs. Fine iron silicide composites containing nanosheets have been obtained by the reaction of $CaSi_2$ and $FeCl_2$ in the molar ratio of 1:1 (the molar ratio of Si/Fe is 2:1).[10),32] Based on these researches, we expect that by decreasing $FeCl_2$ amount, unreacted $CaSi_2$ reacts with additional NaCl to form Na, which could dissolve in molten NaCl–$CaCl_2$ salts ($CaCl_2$ is formed from the reaction of $CaSi_2$ and $FeCl_2$) to form Na–NaCl–$CaCl_2$ liquid phase. And then Si dissolved in Na–NaCl–$CaCl_2$ liquid phase probably reacts with iron silicide (Fe_3Si and FeSi) to form β-$FeSi_2$. Additionally, for Fe–Si system, the Fe/Si supply ratio and thermal treatment condition dependences for the phase selection have been examined, and the silicide phase control and the multiple phase formation of the Fe-silicides have been reported.[33)–38] Therefore, decreasing $FeCl_2$ amount means that the molar ratio of Si/Fe is higher than 2:1, probably contributing to the formation of Si-rich phase (β-$FeSi_2$). Hence, in present study, the impact of the molar ratio of $CaSi_2$ and $FeCl_2$ and additional NaCl on the formation of β-$FeSi_2$ was emphasized on.

2. Experimental procedure

2.1 Material preparation

$CaSi_2$ (99 %), $FeCl_2$ (99.9 %), and NaCl (99.9 %) used in this study are high purity chemicals from Kojundo Chemical Lab. Co., Ltd. in Japan. $CaSi_2$, $FeCl_2$ and NaCl powders were weighted in molar ratio of 1:0.5:2.2, 1:0.75:2.2 and 1:1:2.2, respectively, and named F-0.5, F-0.75 and F-1, respectively. The molar ratio of $CaSi_2$/NaCl was fixed while the molar ratio of $CaSi_2/FeCl_2$ ($x_{CaSi_2/FeCl_2}$) was changed between 1 and 2 ($x_{CaSi_2/FeCl_2}$ = 1–2), which means that the molar ratio of Si/Fe is between 2:1 to 4:1. The weighted powders were ground by a corundum mortar and pestle for 1 min, put into a glass quartz tube, and then sealed in stainless-steel cell under Ar atmosphere with the detected oxygen level of less than 0.1 %. The cells were annealed at 850 °C for 1–3 h in furnace with a heating rate of 10 °C/min from room temperature to 850 °C. After heating, the heaters were turned off, and then samples were naturally cooled in furnace. In addition, the mixture of $CaSi_2$ and NaCl powders in molar ratio of 1:2.2 (named F-0) was prepared and annealed at 850 °C for 1 h. After annealing, the treated samples were immersed in deionized water for 1 h under mild stirring to remove chlorides, and then filtrated, washed another three times by deionized water and one time by ethanol, and dried in air overnight.

2.2 Sample characterization

Phases of samples were characterized by Rigaku X-ray powder diffraction (XRD) operated at 40 kV and 20 mA with Cu Kα radiation in the range of 5–80° with a step of 0.02°. The morphological and structural properties of the nanosheet bundles were characterized by field-emission scanning electron microscopy (SEM: JEOL JSM-7001F) with energy dispersion spectroscopy (EDS), conventional transmission electron microscopy (TEM: JEOL JEM 2100F), high-resolution TEM (HRTEM), and scanning transmission electron microscopy (STEM) with EDS. For the TEM sample preparation, the products were dispersed in a small amount of ethanol, then transferred onto a lacey carbon-coated copper grid and dried.

3. Results

Figure 1 presents XRD patterns of samples F-0.5, F-0.75 and F-1 after annealing at 850 °C for 1 h and washing.

Table 1. The molar ratio of various samples

Sample	$CaSi_2$	$FeCl_2$	NaCl
F-1	1	1.00	2.2
F-0.75	1	0.75	2.2
F-0.5	1	0.50	2.2
F-0	1	—	2.2

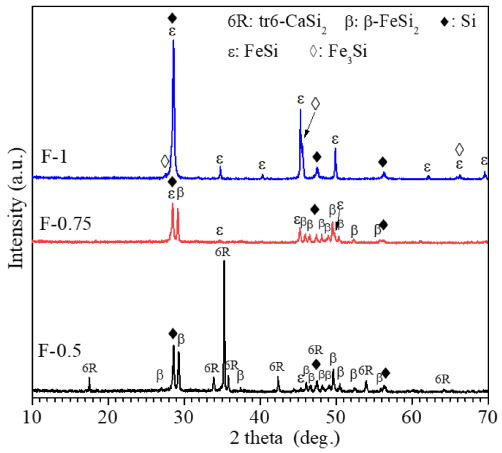

Fig. 1. XRD patterns of samples F-0.5, F-0.75 and F-1 after annealing at 850 °C for 1 h and washing.

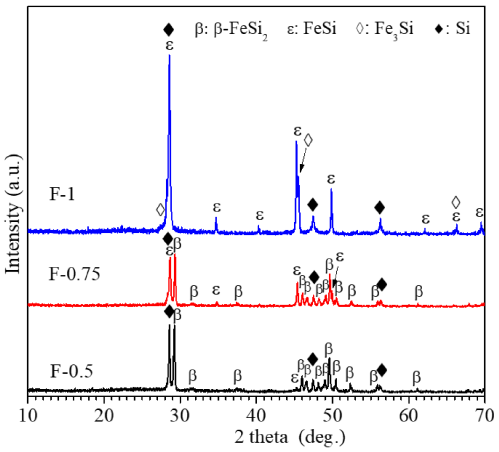

Fig. 2. XRD patterns of samples F-0.5, F-0.75 and F-1 after annealing at 850 °C for 3 h and washing.

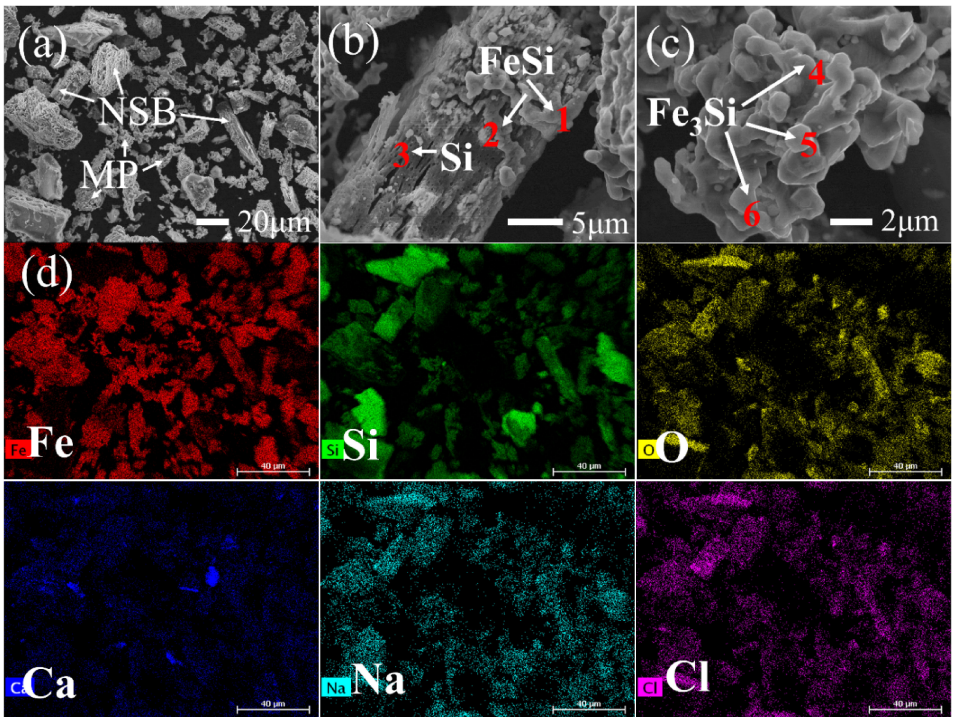

Fig. 3. (a, b, c) SEM images and (d) EDS mappings of the sample F-1 after annealing at 850 °C for 3 h and washing (NSB: nanosheet bundles; MP: microsized particles).

Diffraction peaks corresponding to Si, FeSi, and Fe_3Si were detected in the sample F-1. On the other hand, diffraction peaks of β-$FeSi_2$ were observed in samples F-0.75 and F-0.5. Specifically, diffraction peaks related to β-$FeSi_2$, FeSi and Si were observed in the sample F-0.75. Diffraction peaks of β-$FeSi_2$, tr6-$CaSi_2$ (a crystal structure of $CaSi_2$), Si and a small peak of FeSi were detected in the sample F-0.5. These results illustrate that the formation of β-$FeSi_2$ is favored when $x_{CaSi_2/FeCl_2}$ is larger than 1.

Figure 2 shows XRD patterns of samples F-0.5, F-0.75 and F-1 after annealing at 850 °C for 3 h and washing. Si, FeSi, and Fe_3Si peaks were observed in the sample F-1. By contrast, β-$FeSi_2$ peaks were detected in samples F-0.75 and F-0.5. For example, β-$FeSi_2$, FeSi, and Si peaks were observed in the sample F-0.75. Peaks of β-$FeSi_2$, Si and a small peak of FeSi were observed in the sample F-0.5. Tr6-$CaSi_2$ peaks disappeared in the sample F-0.5 when extended annealing time from 1 h (Fig. 1) to 3 h (Fig. 2), which suggests that $CaSi_2$ could react with NaCl as the previous report.[31] These results also demonstrate that the generation of β-$FeSi_2$ is favorable when $x_{CaSi_2/FeCl_2}$ is larger than 1.

Figure 3 presents microstructure of the sample F-1 after annealing at 850 °C for 3 h and washing. **Table 2** lists EDS results in Fig. 3. As shown in Fig. 3(a), nanosheet bundles and microsized particles can be clearly identified in the sample F-1. It can be seen from EDS mappings [Fig. 3(d)] that Fe and Si were detected on the nanosheet

bundles, suggesting the formation of iron silicide on the surface of Si nanosheet bundles. Based on the EDS spot analysis (Table 2), FeSi (points 1 and 2) was detected on the surface of Si nanosheet bundles [Fig. 3(b)] while Fe_3Si (points 4, 5 and 6) was detected on the microsized particles [Fig. 3(c)]. These results illustrate that β-$FeSi_2$ is not formed when $x_{CaSi_2/FeCl_2}$ is equal to 1.

Detailed microstructure of the sample F-0.5 after annealing at 850 °C for 3 h and washing is presented in **Fig. 4**. EDS results of the selected points are listed in **Table 3**. Nanosheet bundles and microsized particles were detected in the sample F-0.5, which is similar to the products of the sample F-1 (Fig. 3). Fe and Si were observed on the surface of nanosheet bundles and microsized particles [Fig. 4(d)]. Based on EDS spot analyses (Table 3), it is confirmed that the microsized particles and the particles grown on the surface of nanosheet bundles are β-$FeSi_2$. Some incomplete particles containing Ca, Si and O were observed [marked with red circles in Fig. 4(a)], which should be related to unreacted $CaSi_2$ phase. The distribution of some Ca was consistent with the distribution of Cl, which can be considered as remained $CaCl_2$ because of inefficient washing. Na was also heterogeneously distributed on the composites and the distribution of Na was consistent with that of Cl, which is considered remained NaCl due to the inefficient washing. These results demonstrate that β-$FeSi_2$ is formed when $x_{CaSi_2/FeCl_2}$ is larger than 1.

Table 2. EDS spot analyses of selected points in Fig. 3 (at %)

Element	1	2	3	4	5	6
Fe	49.88	43.65	1.42	69.91	67.80	69.58
Si	47.87	50.59	74.71	28.26	29.16	28.01
O	2.26	5.76	23.87	1.83	3.05	2.41

Table 3. EDS spot analyses of selected points in Fig. 4 (at %)

Element	1	2	3	4	5	6
Fe	27.00	32.06	29.65	28.89	28.73	30.79
Si	57.55	63.07	58.05	57.05	62.88	60.06
O	15.45	4.86	12.30	14.06	8.39	9.16

Figure 5 presents STEM images, HRTEM and EDS mappings of the nanosheet pieces after exfoliating from the nanosheet bundles in the sample F-1 after annealing at 850 °C for 3 h and washing. EDS mappings indicate that Fe unevenly distributed on the part of surface of nanosheet (nanosized black dots) and the distribution of Fe mainly coincided with Si and O. HRTEM image with an FFT pattern of the nanosized black dot grown on the Si nanosheet [Fig. 5(b)] illustrates that two patterns of β-$FeSi_2$ are superimposed. The plane spacing of about 0.48 and 0.18 nm was observed, which is related to the lattice spacing of $(1\bar{1}1)$ and $(2\bar{4}1)$ lattice planes of β-$FeSi_2$, respectively, according to the diffraction spots indexed in the FFT pattern. The zone axis direction was perpendicular to (110), somewhat inclined. Si nanosheets with exposed Si (111) planes synthesized by extracting Ca atoms from layered $CaSi_2$ have been reported everywhere.[39),40)] Numerous researches[41)–44)] have studied the epitaxial growth of β-$FeSi_2$ layer on Si (111) substrate and reported that (101) β-$FeSi_2$ or (110) β-$FeSi_2$ // (111) Si. In the actual β-$FeSi_2$ crystal, the rotation along an axis by 90° usually occurs. The observation directions of β-$FeSi_2$ were near (101) or

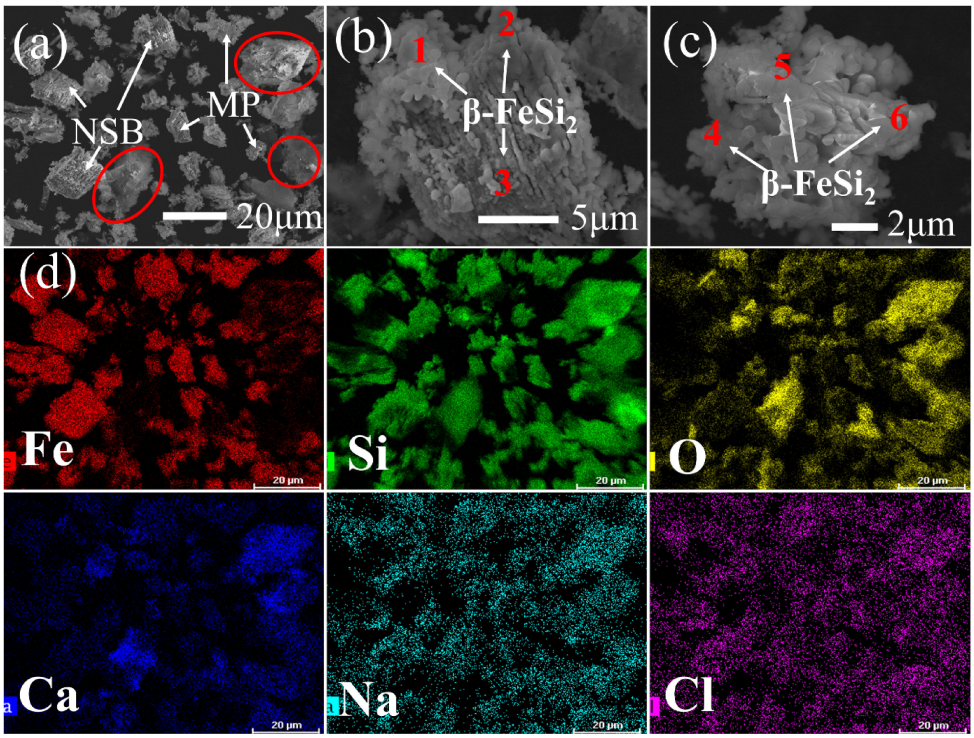

Fig. 4. (a, b, c) SEM images and (d) EDS mappings of the sample F-0.5 after annealing at 850 °C for 3 h and washing (NSB: nanosheet bundles; MP: microsized particles).

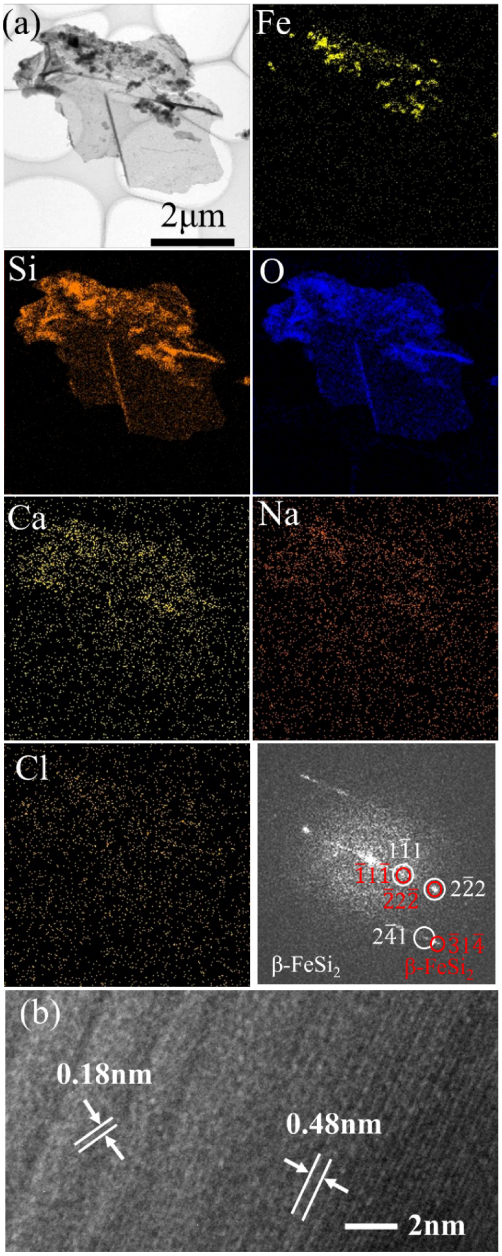

Fig. 5. (a) STEM image and EDS mappings of a piece of nanosheet after exfoliating from the sample F-0.5 annealed at 850 °C for 3 h, and (b) HRTEM and its FFT pattern of black dot.

(110), which is nearly parallel to the sheet surface. This closely agree with the epitaxial relationship (101) or (110) β-$FeSi_2$ // (111) Si. The existence of such growth variants shows that the β-$FeSi_2$ nanoparticles were epitaxially grown on the crystalline Si nanosheets.

The Si and O around β-$FeSi_2$ nanoparticles may be related to amorphous SiO_x. In addition, the distribution of Ca and Na found on the nanosheet was consistent with Cl, which can be considered that $CaCl_2$ and NaCl remained around the nanosheets by insufficient washing. The TEM results illustrate that β-$FeSi_2$ was also formed on the surface of nanosheets of the nanosheet bundles in the sample F-0.5 after annealing at 850 °C for 3 h.

4. Discussion

As shown in Figs. 1 and 2, Si, FeSi and Fe_3Si were formed in the sample F-1 after annealing at 850 °C for 1 and 3 h. By contrast, β-$FeSi_2$ was formed in samples F-0.5 and F-0.75 after annealing at 850 °C for 1 and 3 h, which illustrates that the formation of β-$FeSi_2$ is favored when $x_{CaSi_2/FeCl_2}$ is higher than 1. It has been reported that $CaSi_2$ can react with $FeCl_2$ in the molar ratio of 1:1.[10] Compared with the sample F-1, unreacted $CaSi_2$ in samples F-0.5 and F-0.75 could further react with NaCl to form Na in the heating process.[31] Therefore, the formed Na dissolved in molten NaCl–$CaCl_2$ salts to form Na–NaCl–$CaCl_2$ liquid phase in samples F-0.5 and F-0.75 probably contributes to the formation of β-$FeSi_2$.

It can be seen from **Fig. 6**(a) that starting $CaSi_2$ consists of tr3-$CaSi_2$, tr6-$CaSi_2$, and less amount of Si. Tr6-$CaSi_2$ peaks and a weak Si peak were detected in $CaSi_2$ after annealing at 850 °C for 1 h. $CaSi_2$ has a trigonal structure and contains two polymorphs (tr3-$CaSi_2$ and tr6-$CaSi_2$) at atmosphere pressure based on the stacking of Ca layers. The stacking of trigonal Ca layers follows an ABC sequence with a three-layer repeat distance in the tr3 structure and follows an AABBCC sequence with a six-layer repeat distance in the tr6 structure.[45] Tr6-$CaSi_2$ is more stable than tr3-$CaSi_2$, and tr6-$CaSi_2$ stabilizes over tr3-$CaSi_2$ with higher temperature according to the calculated Gibbs free energy.[46] Therefore, tr3-$CaSi_2$ transformed into tr6-$CaSi_2$ in the heating process. Strong Si peaks were observed in the sample F-1, which illustrate that $CaSi_2$ can react with NaCl at 850 °C. Unreacted $CaSi_2$ in the sample F-0.5 disappeared after prolonging annealing time from 1 h (Fig. 1) to 3 h (Fig. 2) also illustrating that $CaSi_2$ can react with NaCl at 850 °C.

Noted in Fig. 6(b), tr6-$CaSi_2$, Si, $CaCl_2$, NaCl, NaO_3 and NaO_2 peaks were observed in the sample F-0 after annealing at 850 °C for 1 h before washing. The eroded glass quartz tube (the insert image) and the generated oxidized sodium (NaO_3 and NaO_2) demonstrate the formation of Na. The products of F-0 were consistent with the reaction formula: $CaSi_2 + NaCl \rightarrow 2Si + CaCl_2 + 2Na$ in previous report.[31] The eroded glass quartz tube below sample height was probably because of the reaction of glass and Na dissolved in molten $CaCl_2$–NaCl salts, and the eroded glass quartz tube above sample height may be related to Na vapor reacted with glass, which is due to the higher vapor pressure of Na at high temperatures, for example, the vapor pressure of Na at 827 °C (1100 K) and 927 °C (1200 K) is 0.21 and 1 bar,[47] respectively. These results confirmed that $CaSi_2$ can react with NaCl to form Na.

Figure 7 presents the microstructure of the sample F-0 after annealing at 850 °C for 1 h and washing. Porous particles were observed in the sample F-0. Based on the EDS mappings [Fig. 7(d)], these porous particles were mainly Si. Some unreacted $CaSi_2$ particles were also detected [Fig. 7(c)], which is consisted with XRD results in Fig. 6. These unreacted $CaSi_2$ particles were incomplete and had

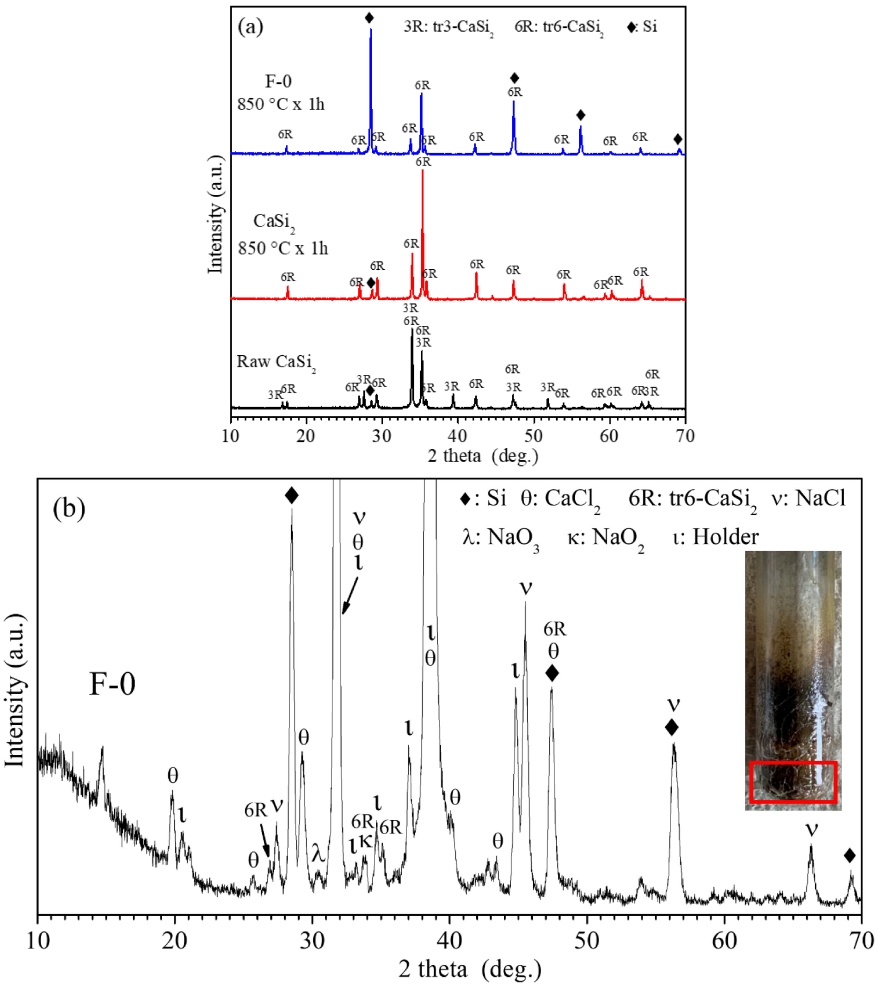

Fig. 6. (a) XRD patterns of raw $CaSi_2$, and raw $CaSi_2$ and the sample F-0 after annealing at 850 °C for 1 h and washing, and (b) XRD patterns and appearance of glass quartz tube (insert image, the red rectangle represents the height of sample) of the sample F-0 after annealing at 850 °C for 1 h before washing.

porous silicon on the surface. Si nanosheet bundles obtained by the reaction of $CaSi_2$ and chlorides have been reported everywhere[6),7),10)–14)] because of Ca is extracted from $CaSi_2$ by chlorides. However, the morphology of porous Si particles formed by the reaction of $CaSi_2$ and NaCl were different from Si nanosheet bundles in previous reports. Similarly, incomplete unreacted $CaSi_2$ particles were observed in the sample F-0.5 after annealing at 850 °C for 3 h [Fig. 4(a)]. By contrast, those Si nanosheet bundles with β-$FeSi_2$ grown on the surface are relatively intact. MacCaldin et al.[48)] reported that the solubility of Si in Na melt at 800 °C was estimated to be 10–20 atomic %. The formation of porous Si particles and incomplete unreacted $CaSi_2$ particles suggests that Si can dissolve in Na–NaCl–$CaCl_2$ liquid phase, especially for the Si generated form the reaction of $CaSi_2$ and NaCl.

Figure 8 presents XRD patterns and appearance of glass quartz tube of samples F-0.5, F-0.75 and F-1 after annealing at 850 °C for 3 h before washing. Oxidized sodium peaks were observed in samples F-0.5 (NaO_3 and NaO_2) and F-0.75 (NaO_3) and the glass tubes of samples F-0.5 and F-0.75 were eroded. These results demonstrate that Na generated in samples F-0.5 and F-0.75. On the other hand, no oxidized sodium peaks were detected and the glass quartz tube was not eroded in the sample F-1, which illustrates that Na is not generated in the sample F-1. It has been demonstrated that Si can dissolve in molten NaCl, or $MnCl_2$, or $MgCl_2$ salt around 800 °C, especially in the presence of O_2.[49)] As shown in Figs. 1 and 2, no β-$FeSi_2$ was formed in the sample F-1 after annealing at 850 °C for 1–3 h, illustrating that β-$FeSi_2$ was not generated in molten NaCl–$CaCl_2$ salts in short time (3 h). By contrast, β-$FeSi_2$ was formed in samples F-0.5 and F-0.75, illustrating that β-$FeSi_2$ was formed in Na–NaCl–$CaCl_2$ liquid phase, which is because Si dissolved in Na–NaCl–$CaCl_2$ liquid phase probably more active to react with iron silicide (Fe_3Si and FeSi) grown on the surface of Si nanosheet bundles and microsized particles to form β-$FeSi_2$.

In addition, based on the starting material listed in **Table 1**, the molar ratio of Si/Fe in samples F-0.5, F-0.75 and F-1 was 4:1, 3:1 and 2:1 respectively. Numerous researchers[37),50)] reported that β-$FeSi_2$ film grown on Si substrate were obtained at low temperature (530 or 630 °C)

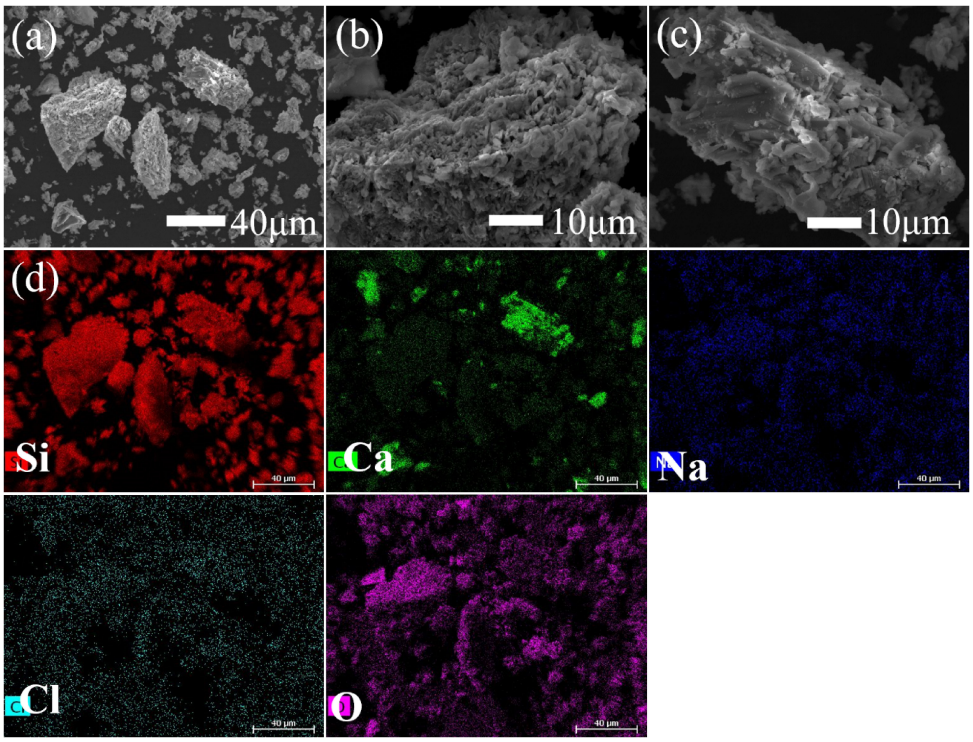

Fig. 7. (a, b, c) SEM images and (d) EDS mappings of the sample F-0 after annealing at 850 °C for 1 h and washing.

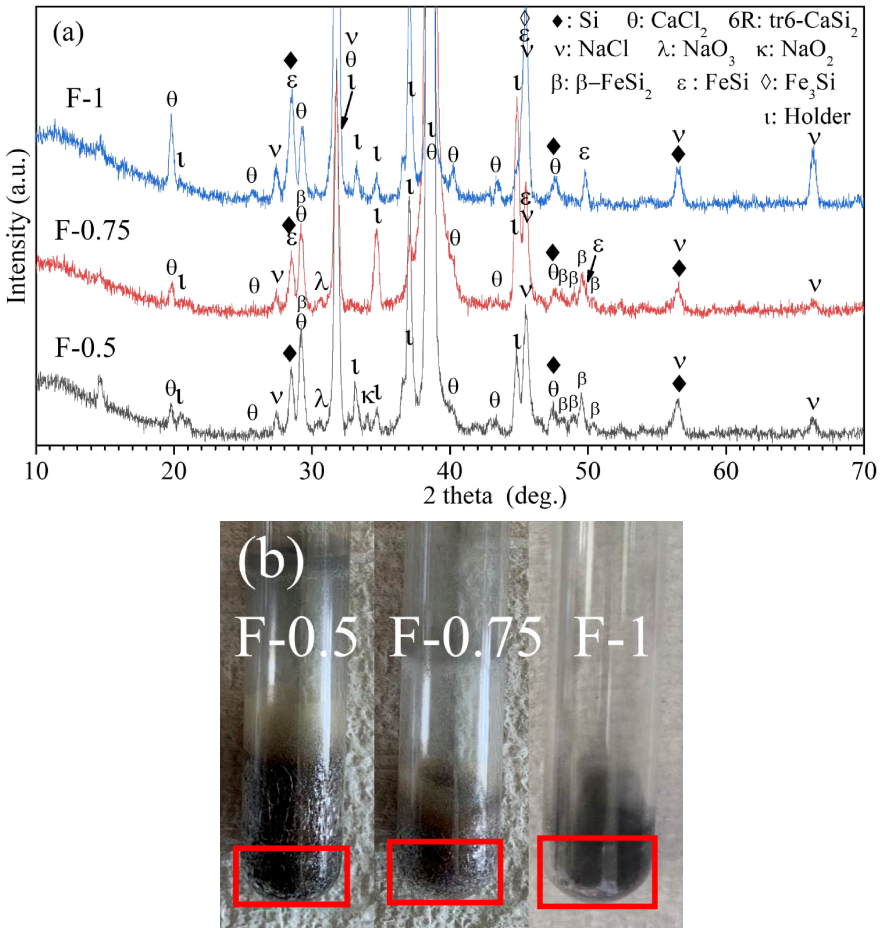

Fig. 8. (a) XRD patterns and (b) appearance of glass quartz tube of samples F-0.5, F-0.75 and F-1 after annealing at 850 °C for 3 h before washing (the red rectangles represent the height of samples).

using Fe–Si co-deposition method (the molar ration Si/Fe is around 2:1). However, it has been reported that peaks of Fe, Si and Fe_3Si were detected after annealing the mixture of Fe powder (< 45 μm) and Si powder (< 70 μm) (the molar ratio of Si/Fe is 2:1) without Na at 800 °C for 24 h in a sealed stainless-steel tube under Ar atmosphere.[27] These results illustrate that the activity and uniformity of nanoscale Si/Fe layer may be different from microsized Si and Fe particles. Theoretically, Si-rich phase could increase the contact area of Si and iron silicide (FeSi and Fe_3Si) and decrease the diffusion distance of Si, which is probably contributed to the formation of β-$FeSi_2$. As shown in Fig. 3, microsized FeSi particles formed on the surface of Si nanosheet bundles [Fig. 3(b)] in the sample F-1 can be called Si-rich phase when compared with Fe_3Si microsized particles [Fig. 3(c)]. However, β-$FeSi_2$ was not formed on the surface of Si nanosheet bundles in the sample F-1 [Fig. 3(b)], although it was annealed at 850 °C for 3 h. This is probably because of the nucleation difficulties of β-$FeSi_2$.[25),26)] Therefore, the main reason for the formation of β-$FeSi_2$ in samples F-0.5 and F-0.75 is because Si dissolved in Na–NaCl–$CaCl_2$ liquid phase react with iron silicide (Fe_3Si and FeSi) grown on the surface of Si nanosheet bundles and microsized particles to form β-$FeSi_2$. As shown in Figs. 4(a) and 7, incomplete unreacted $CaSi_2$ particles [Fig. 4(a)] and porous Si (Fig. 7) indicate that Si generated by the reaction of $CaSi_2$ and NaCl may be more soluble in Na–NaCl–$CaCl_2$ liquid phase, which protects the Si nanosheet bundles with β-$FeSi_2$ layer on the surface (Fig. 4).

Noted in Fig. 5, nanosized β-$FeSi_2$ particles grown on the surface of Si nanosheet bundles was consisted with the epitaxial relationship of (101) or (110) β-$FeSi_2$ // (111) Si. Numerous researchers[25),26),42),51)] reported that epitaxial growth of β-$FeSi_2$ film on Si (111) substrate by depositing a few nanometers iron onto a silicon substrate and annealing. In addition, epitaxial growth of β-$FeSi_2$ nanodots (~2 nm high and ~8 nm wide) on Si (111) substrate were obtained by depositing Fe on Si nanodots on oxidized Si (111) surfaces and annealing.[52)] Therefore, the nanosized β-$FeSi_2$ grown on the Si (111) nanosheet was probably because Si diffused from Si (111) nanosheet to deposited iron or iron silicide (Fe_3Si and FeSi) nanoparticles to form β-$FeSi_2$.

5. Conclusion

The influence of the molar ratio of $CaSi_2$ and $FeCl_2$ powders and additional NaCl on the formation of β-$FeSi_2$ under Ar atmosphere were systematically studied in this work. β-$FeSi_2$/Si composites (β-$FeSi_2$ grown on the surface Si nanosheet bundles and the surface of Si nanosheets) were formed in the sample with a 1:0.5:2.2 molar ratio of $CaSi_2$, $FeCl_2$ and NaCl. The formation of β-$FeSi_2$ was favored in the sample with a molar ratio of $CaSi_2/FeCl_2$ higher than 1, whereas β-$FeSi_2$ was not formed in the sample with a molar ratio of $CaSi_2/FeCl_2$ equal to 1. This is because unreacted $CaSi_2$ in the sample with a molar ratio of $CaSi_2/FeCl_2$ higher than 1 could react with NaCl to form Na and then dissolve in molten NaCl–$CaCl_2$ salts to form Na–NaCl–$CaCl_2$ liquid phase. Si dissolved in Na–NaCl–$CaCl_2$ liquid phase should be more active to react with iron silicide (Fe_3Si and FeSi) to form β-$FeSi_2$.

References

1) L. Sun, B. Wang and Y. Wang, *Adv. Mater. Interfaces*, 5, 1701300 (2018).
2) L. Sun, B. Wang and Y. Wang, *Appl. Surf. Sci.*, 473, 641–648 (2019).
3) Z. Hu, Z. Chen, J. Huang, M. Yan, M. Zhang, L. Zhang, X. Li and Z. Feng, *CrystEngComm*, 22, 4074–4078 (2020).
4) Z. Hu, L. Zhang, J. Huang, Z. Feng, Q. Xiong, Z. Ye, Z. Chen, X. Li and Z. Yu, *Nanoscale*, 13, 8264–8274 (2021).
5) C. Qian, W. Sun, D. L. Hung, C. Qiu, M. Makaremi, S. G. H. Kumar, L. Wan, M. Ghoussoub, T. E. Wood and M. Xia, *Nat. Catal.*, 2, 46–54 (2019).
6) H. Imagawa, N. Takahashi, T. Nonaka, Y. Kato, K. Nishikawa and H. Itahara, *J. Mater. Chem. A*, 3, 9411–9414 (2015).
7) S.-Y. Oh, H. Imagawa and H. Itahara, *J. Mater. Chem. A*, 2, 12501–12506 (2014).
8) T. Xiang, Z. Chen, Z. Rao, M. Yan, Z. Feng, X. Li, H. Yang, J. Huang and X. Shen, *Ionics*, 27, 3663–3669 (2021).
9) M. Yamamoto, M. Takahashi, Y. Terauchi, Y. Kobayashi, S. Ikeda and A. Sakuda, *J. Ceram. Soc. Jpn.*, 125, 391–395 (2017).
10) H. Itahara, T. Kobayashi, T. Ohsuna, T. Asaoka and Y. Saito, 12th IEEE Int. Conf. on Nanotechnology (IEEE-NANO), Birmingham, UK (2012) pp. 1–4.
11) S. Y. Oh, H. Imagawa and H. Itahara, *Chem.-Asian J.*, 9, 3130–3135 (2014).
12) H. Itahara, S.-Y. Oh, T. Yamada and H. Yamane, *J. Appl. Phys.*, 56, 05DE01 (2017).
13) H. Imagawa and H. Itahara, *Dalton T.*, 46, 3655–3660 (2017).
14) Y. Huang, R. Tamaki, P. Yuan, Y. Kumazawa, N. Atsumi, V. Saxena, N. Ahsan, Y. Okada, Y. Hayakawa and H. Tatsuoka, *J. Appl. Phys.*, 58, SBBK04 (2019).
15) H.-Y. Lee and S.-M. Lee, *J. Power Sources*, 112, 649–654 (2002).
16) Y. Domi, H. Usui, Y. Shindo, S. Yodoya, H. Sato, K. Nishikawa and H. Sakaguchi, *Electrochemistry*, 88, 548–554 (2020).
17) Y. Chen, J. Qian, Y. Cao, H. Yang and X. Ai, *ACS Appl. Mater. Inter.*, 4, 3753–3758 (2012).
18) H. Usui, K. Nouno, Y. Takemoto, K. Nakada, A. Ishii and H. Sakaguchi, *J. Power Sources*, 268, 848–852 (2014).
19) J. Liu and X. W. Liu, *Adv. Mater.*, 24, 4097–4111 (2012).
20) J.-i. Tani and H. Kido, *J. Appl. Phys.*, 86, 464–467 (1999).
21) P. Vaqueiro and A. V. Powell, *J. Mater. Chem.*, 20, 9577–9584 (2010).
22) Y. Zhang and D. Ivey, *J. Mater. Sci.*, 33, 3131–3135 (1998).
23) R. Walser and R. Bene, *Appl. Phys. Lett.*, 28, 624–625 (1976).

24) A. L. Schmitt, J. M. Higgins, J. R. Szczech and S. Jin, *J. Mater. Chem.*, 20, 223–235 (2010).
25) N. Baldwin and D. Ivey, *J. Mater. Sci.*, 31, 31–37 (1996).
26) K. Radermacher, S. Mantl, C. Dieker, H. Lüth and C. Freiburg, *Thin Solid Films*, 215, 76–83 (1992).
27) T. Yamada and H. Yamane, *Chem. Mater.*, 19, 6047–6051 (2007).
28) T. Yamada and H. Yamane, *J. Alloy. Compd.*, 509, L23–L25 (2011).
29) F. Kawamura, H. Yamane, T. Yamada, S. Yin and T. Sato, *J. Ceram. Soc. Jpn.*, 115, 74–76 (2007).
30) T. Yamada and H. Yamane, *Phys. Status Solidi C*, 10, 1692–1695 (2013).
31) M. Harada, T. Mori, N. Goda and A. Iyama, Patent, JPWO2017175518A1 (2018).
32) Y. Li, Y. Shimura, L. Chen, J. Ansari and H. Tatsuoka, Submited to journal (2022).
33) N. Dahal and V. Chikan, *Chem. Mater.*, 22, 2892–2897 (2010).
34) J. H. Won, K. Sato, M. Ishimaru and Y. Hirotsu, *Jpn. J. Appl. Phys.*, 46, 732–737 (2007).
35) V. V. Balashev, V. V. Korobtsov, T. A. Pisarenko, E. A. Chusovitin and V. A. Vikulov, *e-J. Surf. Sci. Nanotechnol.*, 5, 136–142 (2007).
36) A. Tiwari, R. Gupta, F. Singh, M. Gupta, V. Reddy, G. Sharma and A. Gupta, *Vacuum*, 180, 109546 (2020).
37) I. Tarasov, M. Visotin, A. Aleksandrovsky, N. Kosyrev, I. Yakovlev, M. Molokeev, A. Lukyanenko, A. Krylov, A. Fedorov and S. Varnakov, *J. Magn. Magn. Mater.*, 440, 144–152 (2017).
38) U. Starke, W. Weiss, M. Kutschera, R. Bandorf and K. Heinz, *J. Appl. Phys.*, 91, 6154–6161 (2002).
39) X. Meng, H. Imagawa, E. Meng, H. Suzuki, Y. Shirahashi, K. Nakane, H. Itahara and H. Tatsuoka, *J. Ceram. Soc. Jpn.*, 122, 618–621 (2014).
40) X. Meng, K. Sasaki, K. Sano, P. Yuan and H. Tatsuoka, *Jpn. J. Appl. Phys.*, 56, 05DE02 (2017).
41) M. Takauji, N. Seki, T. Suemasu, F. Hasegawa and M. Ichida, *J. Appl. Phys.*, 96, 2561–2565 (2004).
42) J. E. Mahan, V. L. Thanh, J. Chevrier, I. Berbezier, J. Derrien and R. G. Long, *J. Appl. Phys.*, 74, 1747–1761 (1993).
43) N. Cherief, C. D'Anterroches, R. Cinti, T. Nguyen Tan and J. Derrien, *Appl. Phys. Lett.*, 55, 1671–1673 (1989).
44) S. Lagomarsino, F. Scarinci, C. Giannini, P. Castrucci, G. Savelli, J. Derrien, J. Chevrier, V. Le Thanh and M. Grimaldi, *J. Vac. Sci. Technol. B*, 9, 2433–2436 (1991).
45) K. D. Sattler, "Silicon Nanomaterials Sourcebook: Low-Dimensional Structures, Quantum Dots, and Nanowires, Volume One", Vol. 1, CRC Press (2017).
46) R. Nedumkandathil, D. E. Benson, J. Grins, K. Spektor and U. Häussermann, *J. Solid State Chem.*, 222, 18–24 (2015).
47) I. Barin and G. Platzki, "Thermochemical data of pure substances", 3rd ed., VCH, New York (1995) pp. 200–1880.
48) J. McCaldin, M. Little and A. Widmer, *J. Phys. Chem. Solids*, 26, 1119–1123 (1965).
49) J. Ansari, F. Komeda, S. Ito, R. Ogino and R. Yamamoto, private commutation.
50) K. Watanabe, T. Taniguchi, S. Sakane, S. Aoki, T. Suzuki, T. Fujita and Y. Nakamura, *Jpn. J. Appl. Phys.*, 56, 05DC04 (2017).
51) Z. Liu, S. Wang, N. Otogawa, Y. Suzuki, M. Osamura, Y. Fukuzawa, T. Ootsuka, Y. Nakayama, H. Tanoue and Y. Makita, *Sol. Energ. Mat. Sol. C.*, 90, 276–282 (2006).
52) Y. Nakamura, Y. Nagadomi, S.-P. Cho, N. Tanaka and M. Ichikawa, *Phys. Rev. B*, 72, 075404 (2005).